J. Phys. IV France **116** (2004) 211-217

DOI: 10.1051/jp4:2004116008

Hydrodynamic clouds and Bose-Einstein condensation

Ch. Buggle, I. Shvarchuck*, W. von Klitzing and J.T.M. Walraven

FOM-Institute for Atomic and Molecular Physics, Kruislaan 407, 1098 SJ Amsterdam

Abstract. We discuss the characterization of dense elongated clouds of ^{87}Rb in the context of the process of Bose-Einstein condensation under hydrodynamic conditions. The condensation is induced by shock-cooling of thermal clouds. This gives rise to strong temperature gradients and results in a non-equilibrium shape of the (quasi)condensate with strong phase fluctuations just after formation.

1. INTRODUCTION

Almost a decade after the first observation of Bose-Einstein condensation in atomic gases [1, 2] much remains to be learned about the processes that transform a classical thermal gas into a coherent macroscopic quantum object, the condensate. To study condensate formation one typically starts with a thermal cloud, carefully prepared under equilibrium conditions just above the critical temperature [3–5]. Extracting heat, the gas is pulled out of equilibrium and after some time the condensate will nucleate and grow. Unlike classical growth, condensate formation involves not only a kinetic stage but also a coherent stage. This reflects the Bose statistics, which favor scattering into quantum states that are already occupied. Aside from the occupation the phase properties should also be considered. In particular for elongated condensates phase fluctuations can persist long after the condensate has formed. Thus different characteristic times are to be distinguished for nucleation, growth, and phase relaxation [6].

In this contribution we discuss some phenomena typical for condensate formation in dense elongated clouds. The high column density gives rise to hydrodynamic behavior. This differs in several aspects from the familiar behavior of collisionless thermal clouds, affecting both static and dynamic properties [7–14]. We discuss how the expansion behavior and time-of-flight thermometry are affected [13, 14]. Further, we discuss how temperature gradients give rise to the formation of condensates in non-equilibrium shapes [5].

2. CHARACTERIZING HYDRODYNAMIC THERMAL CLOUDS

In Amsterdam [5, 14], we prepare our samples by loading a magneto-optical trap with approximately 10^{10} atoms from the ^{87}Rb source described in [15]. After optical pumping to the $|S_{1/2}, F = 2, m_F = 2\rangle$ state typically 4×10^9 atoms are captured in a Ioffe-Pritchard quadrupole magnetic trap with axial frequency $\omega_z/2\pi = 20.8(1)$ Hz and radial frequency $\omega_\rho/2\pi = 477(2)$ Hz, respectively. Then, the gas is compressed and evaporatively cooled to a temperature just above T_C. This yields a cloud of $N = 3.5(3)\times10^6$ atoms at density $n_0 = 3.6(6)\times10^{14}$ cm^{-3} in the trap center and temperature $T_0 = 1.17(5)\,\mu$K, corresponding to a degeneracy (fugacity) of $D = 0.95(4)$.

To arrive at these numbers we have to go beyond the standard time-of-flight analysis for collisionless clouds [16]. The procedure is illustrated in Fig.1 . The absorption image taken at 10.3 ms of expansion is shown in Fig.1a. The optical density is related to the column density $n_2(z, \rho)$ of an initially harmonically

Present address: Fisher & Paykel Healthcare, PO Box 14348, Panmure, Auckland, New Zealand

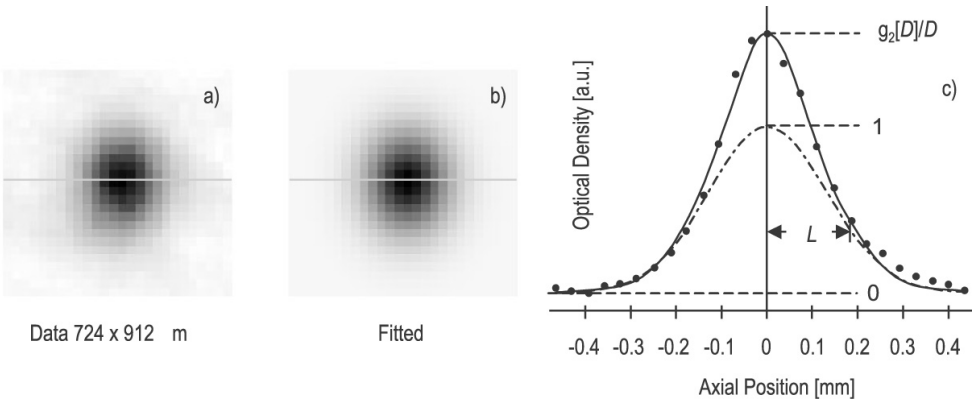

Figure 1. a) Time-of-flight absorption image; b) The function $n_2(z,\rho)$ after fitting, plotted as optical density. c) Axial profile of column density showing the fit result for $D = 0.98$ and $L = 18$ mm (solid line). The dash-dotted line corresponds to a gaussian profile with the same axial size L.

confined Bose gas. Presuming scaling of the cloud shape during the expansion, this can be written as (see e.g. [16])

$$n_2(z,\rho) = n_{20} g_2[De^{-[z/L]^2-[\rho/R]^2}]/g_2[D], \tag{2.1}$$

where n_{20} is the peak column density and the Bose enhancement is expressed by the g_2 function, defined by $g_a[x] = \sum_{l=1}^{\infty} x^l/l^a$. The parameters $L(t)$ and $R(t)$ define the axial and radial sizes at expansion time t; D is the degeneracy of the cloud. We obtain Fig.1b by fitting Eq.(2.1) to the data. In Fig.1c we show the column density profile along the symmetry axis. The solid line in Fig.1c corresponds to a Bose distribution with $D = 0.98$. The dashed line represents a gaussian with the same L. In this case the central Bose-enhancement is $g_2[D]/D = 1.55$.

For short expansion times ($t \ll 1/\omega_z$) , the initial axial size is observed, $L(t) \simeq L(0) \equiv L_0$, and the temperature T_0 follows with

$$\tfrac{1}{2} m\omega_z^2 L_0^2 = kT_0 + E_{\rm mf}, \tag{2.2}$$

where $E_{\rm mf} = g\int n^2(\mathbf{r})d\mathbf{r}/\int n(\mathbf{r})d\mathbf{r}$ with $g = (4\pi\hbar^2/m)a$ the interaction coupling constant [12–14][1]. Introducing $\xi \equiv E_{\rm mf}/(kT_0 + E_{\rm mf})$, we can rewrite Eq.(2.2) as $\frac{1}{2}m(1-\xi)\omega_z^2 L_0^2 = kT_0$. Hence, the effect of the mean field is to 'dress' the trapping potential, broadening the density distribution to yield a slightly lower effective frequency. The central density in the cloud follows with $n_0 = g_{3/2}[D]/\Lambda_0^3$, where $\Lambda_0 = (2\pi\hbar^2/mkT_0)^{1/2}$ is the thermal wavelength. Even at the relatively high densities discussed here, the mean field correction remains small, $\xi \approx 0.03$, and results only in small corrections of T_0 and n_0. The total atom number is given by

$$N = \beta_0^4 g_3[D]\left(\frac{m\,\bar{\omega}}{2\hbar}\right)^3 L_0^6, \tag{2.3}$$

where $\beta_0 = R_0/L_0 = \omega_z/\omega_\rho$ is the aspect ratio and $\bar{\omega} = (\omega_\rho^2\omega_z)^{1/3}(1-\xi)^{1/2}$ the mean dressed trap frequency. Note that, just above $T_{\rm C}$, knowledge of the optical absorption cross section is *not* required to determine the total atom number[2]. In this case the accuracy of N is limited by the experimental error in D.

[1] This expression is correct to first order in the mean field correction, presuming the cloud *shape* to remain ideal-gas-like.

[2] In the classical limit $g_3[D] \simeq D$ and the Bose-enhancement factor $g_2[D]/D$ differs too little from unity to extract a value for D from only the shape of the $n_2(z,\rho)$ fit. In this case the total atom number is determined with $N = n_{20}\pi L_0 R_0$ and, hence, requires knowledge of the optical cross section.

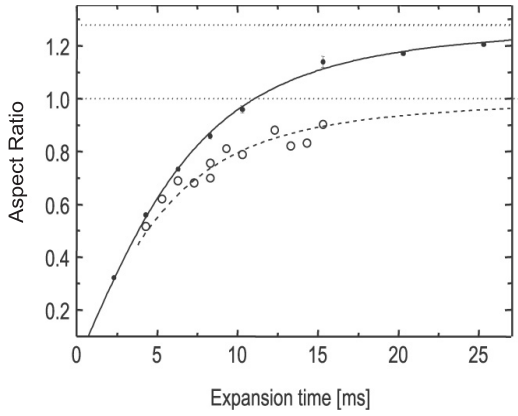

Figure 2. Aspect ratio $\beta(t) = R(t)/L(t)$ as a function of expansion time t. The solid dots are obtained for the hydrodynamic clouds discussed in the text. The open circles correspond to collisionless clouds.

Although the interaction effects are too weak to sizeably broaden the thermal distribution, they strongly affect the expansion behavior of dense thermal clouds: as opposed to the collisionless case, dense elongated clouds expand anisotropically (see Fig.2). When the collisional mean free path is less than the smallest characteristic size of a cloud, pressure gradients will drive the expansion hydrodynamically [7, 9]. Therefore, dense elongated clouds display an increased expansion velocity in the radial direction. Because the density drops rapidly, the gas becomes collisionless before a hydrodynamic kick can develop in the axial direction. The increase of the radial expansion velocity goes at the expense of the gas temperature, i.e. the gas cools isentropically to a temperature $T_* < T_0$. This results in a decrease of axial expansion velocity as compared to that of a collisionless cloud at the same temperature [13, 14].

The anisotropy of expansion has important consequences for time-of-flight thermometry. In cases where the axial and radial asymptotic expansion velocities v_z and v_ρ, corresponding to the effective temperatures T_z and T_ρ, are known[3], T_0 can be calculated with [14][4]

$$\tfrac{3}{2}T_0(1 + \tfrac{2}{3}\xi) = \tfrac{1}{2}T_z + T_\rho. \tag{2.4}$$

However, even single shot time-of-flight information is sufficient to calculate all three temperatures including hydrodynamic and mean field effects. For intermediate expansion times t, when the radial expansion velocity has reached its asymptotic value, T_ρ is known as is the aspect ratio $\beta(t) = R(t)/L(t) \gtrsim 1$. In such cases the isentropic cooling ratio T_*/T_0 and the ratio T_ρ/T_0 may be estimated by inverting the expression for the aspect ratio given in Ref. [14]

$$\frac{T_*}{T_0} = \frac{3 + 2\xi}{1 + 2\beta^2(t)} - \frac{1}{\omega_z^2(t - t_*)^2}\frac{1}{1 + \beta^{-2}(t)/2}\,; \qquad \frac{T_\rho}{T_0} = \frac{3}{2}\left(1 - \frac{1}{3}\frac{T_*}{T_0}\right) + \xi. \tag{2.5}$$

Here $t_* \equiv (1/\omega_\rho)[(T_0/T_*)^{3/2} - 1]^{1/2}$ is the characteristic time after which the expansion is collisionless. The solid line in Fig.2 corresponds to $t_* \approx 0.3$ ms, $\xi = 0.03$, $T_*/T_0 = 0.71$ and $T_\rho/T_0 = 1.15$, fitting the expression for the aspect ratio given in Ref. [14]. With the measured $T_\rho = 1.35\ \mu$K we obtain

[3]The asymptotic expansion velocities are defined as $v_z(t) \equiv \dot{L}(t)$ and $v_\rho(t) \equiv R(t)$, and are related to the effective temperatures through $v_i = \lim_{t\to\infty} v_i(t) = (2k_BT_i/m)^{1/2}$, with $i \in \{\rho, z\}$.

[4]This expression is valid under conditions where the thermal motion is only partially converted into directed motion (no collisional hydrodynamic kick in axial direction). The mean field is fully converted into directed motion.

$T_0 = 1.17\,\mu$K. This result can obtained with Eqs.(2.5) after one iteration, starting out with $t_* = 0$ and $\xi = 0$ and the data of a *single* absorption image. Note that the cooling is substantial (29%) although only a few collisions take place before the velocities freeze out at time t_*.

Having established the initial temperature T_0 and the central density n_0 it is straightforward to calculate the mean free path λ_0. For the trap center we find with the usual expression for a uniform gas $\lambda_0 = (\sqrt{2}n_0\sigma)^{-1} \approx 3\,\mu$m [17]. Here $\sigma = 8\pi a^2$ is the elastic scattering cross-section in the s-wave limit with $a = 98.98(4)a_0$ the scattering length [18]. For the highest densities studied in Amsterdam we calculate in the radial direction $\lambda_0/R_0 \approx 0.5$, which corresponds to the cross-over regime between collisionless and hydrodynamic behavior. As evident from Fig.2. even at the onset of hydrodynamic conditions the effects are already quite noticeable.

3. CONDENSATE FORMATION IN HYDRODYNAMIC CLOUDS

Let us now have a look at the consequences of the hydrodynamicity for condensate formation. In collisionless clouds, condensates are typically [1, 2] created by quasi-static growth, with heat extraction limiting the formation rate. This results in equilibrium condensates in the center of the trap, in accordance with the ideal gas picture of a condensate growing from the harmonic oscillator *ground state*. To observe the actual formation process, the heat should be extracted much faster, i.e. on a time scale shorter than the formation time. Since the first experiment on condensate growth, by Miesner *et al.* [3], this is done by fast radio-frequency (rf) removal of the most energetic atoms from the trap (shock cooling). Starting from a thermal gas just above T_C, the condensate appears as the result of thermalization. Miesner *et al.* [3] observed the growth under adiabatic conditions. Köhl *et al.* [4] continued the extraction of heat by evaporating atoms, also during growth. In both experiments, the condensate was observed to grow from the trap center as expected for clouds under close to collisionless conditions [19].

For the experiments in Amsterdam, with $\lambda_0/L_0 \approx 0.02$ in axial direction, the Knudsen criterion for axial hydrodynamicity ($\lambda_0/L_0 \ll 1$) is very well satisfied. The small mean free path allows us to

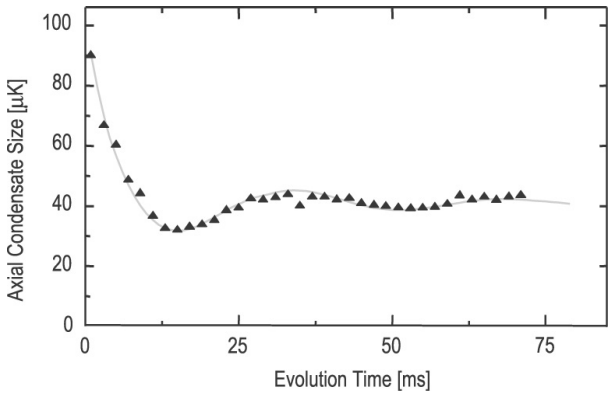

Figure 3. Axial condensate size $L(t)$ as a function of evolution time t for an expansion time of $\tau = 2.8$ ms. The gray line is a guide to the eye and is compatible with a strongly damped quadrupole oscillation.

presume a *local* thermal equilibrium and, hence, the occurrence of axial temperature gradients. As can be seen in Fig.3, shock cooling leads in this case to simultaneous nucleation over a major part of the cloud length and subsequent shape oscillations before equilibrium is reached. The gas is cooled by a brief rf truncation of the trap to a depth of $\varepsilon_{\rm tr} \approx 3\,\mu$K, which removes $\sim 50\%$ of the atoms from the $T_0 = 1.17\,\mu$K cloud. This *truncation stage* has a duration of $t_{\rm tr} = 1$ ms, long enough ($t_{\rm tr} > 1/\omega_\rho$) to allow atoms with radial energy $\varepsilon_\rho > \varepsilon_{\rm tr}$ to escape from the trap, yet short enough to avoid evaporative cooling.

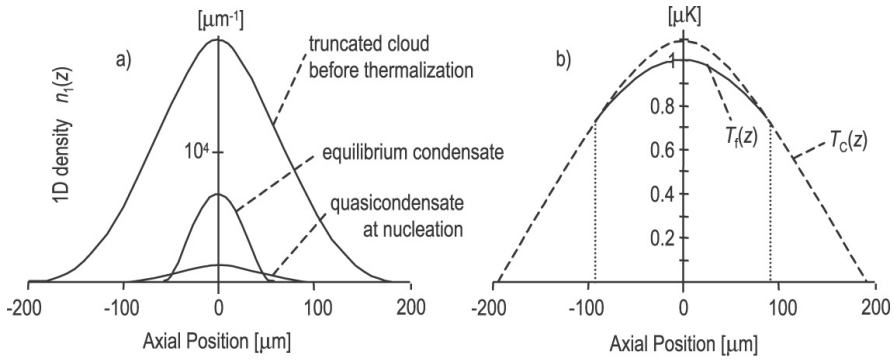

Figure 4. Properties of the hydrodynamic cloud described in section 2: a) 1D axial density distribution for three evolution times: cloud just after truncation; condensate just after nucleation; equilibrium condensate. b) Dashed line: the local distribution $T_C(z)$ for the truncated distribution shown at the left; solid line: the local temperature $T_f(z)$ before global thermalization as calculated with Eq.(3.5). In between the dotted lines the gas will locally Bose condense.

Then, the radio frequency is stepped back up for a variable time t_{th} to allow the gas to thermalize under formation of a condensate. At the end of this *thermalization stage* the trap is switched off and the cloud is analyzed after an expansion time τ by absorption imaging.

To follow the evolution of the trapped gas after truncation we took time-of-flight absorption images for a range of evolution times $t \equiv t_{tr} + t_{th}$ and a fixed expansion time τ. The images show a bimodal distribution, indicating that the truncation procedure results in BEC. The condensate fraction grows to a final value of 6% with a characteristic time of 6 ms. For the shortest expansion time, $\tau = 2.8$ ms ($\tau \ll 1/\omega_z$), the axial size $L(\tau)$ of the condensate is still close to the axial size L_0 of the condensate in the trap, just prior to release. As shown in Fig.3, $L(t)$ initially exceeds the equilibrium length L_∞ by a factor $L_0/L_\infty = 2.2(3)$ and rapidly decreases to reach the equilibrium value after one strongly damped shape oscillation [5].

Knowing the trap potential $\mathcal{U}(z,\rho)$, the truncation energy ε_{tr} and the initial (global) temperature T_0 and degeneracy D, we can use an ideal Bose gas model to estimate the axial density- and temperature-profiles immediately after the gas has (locally) thermalized. In Fig.4a we plot the 1D density distribution just after truncation,

$$n_1(z) = \frac{1}{\Lambda}\left(\frac{kT}{\hbar\bar{\omega}_\rho}\right)^2 g_{5/2}[D(z)] P_{BE}[5/2, \eta(z), D(z)]. \tag{3.1}$$

Here, $P_{BE}[5/2, \eta(z), D(z)]$ is the local Bose-Einstein truncation function[5] with $D(z) = De^{-\mathcal{U}(z)/kT}$ the local fugacity. All atoms with energy $\varepsilon > \varepsilon_{tr}$ are presumed to escape. On the basis of Eq.(3.1) we can calculate the local BEC transition temperature $T_C(z)$, treating the trap locally as a short section of a

[5]The function $P_{BE}[a,\eta,D]$ is defined in analogy with the regularized incomplete gamma functions $P[a,\eta] = \int_0^\eta dX\, X^{a-1}\, e^{-X}/\Gamma(a)$ used to describe truncated gaussian clouds,

$$P_{BE}[a,\eta,D] = \frac{1}{g_a[D]} \sum_{l=1}^{\infty} \frac{D^l}{l^a} P[a, l\eta],$$

where $\eta(z) = [\varepsilon_{tr} - \mathcal{U}(z)]/kT_0$ is the local truncation parameter at position z on the trap axis. $P_{BE}[a,\eta,D]$ increases monotonically, for values of $a > 0$ and $0 < D \leq 1$, from zero at $\eta = 0$ to unity for $\eta \to \infty$.

cylindrically-symmetric radially harmonic trap[6]

$$kT_{\rm C}(z) = \hbar\omega_\rho \left(\frac{2\pi\hbar}{m\omega_\rho}\right)^{1/5} \left(\frac{n_1(z)}{\zeta(5/2)}\right)^{2/5}, \tag{3.2}$$

where $\zeta(n)$ is the Riemann Zeta function. The result is shown as the dashed line in Fig.4b. For the ideal gas it is also straightforward to calculate the local energy per remaining atom along the symmetry axis just after truncation but before local thermalization

$$\frac{E_1(z)}{n_1(z)} = \mathcal{U}(z,0) + \frac{5}{2}kT_0 \frac{g_{7/2}[D(z)]P_{\rm BE}[7/2,\eta(z),D(z)]}{^2g_{5/2}[D(z)]P_{\rm BE}[5/2,\eta(z),D(z)]}. \tag{3.3}$$

With the local energy per remaining atom known, we can estimate the temperature $T_{\rm f}(z)$ presuming local thermalization

$$\frac{E_1(z)}{n_1(z)} = \mathcal{U}(z,0) + \frac{5}{2}kT_{\rm C}\frac{\zeta(7/2)}{\zeta(5/2)}[T_{\rm f}(z)/T_{\rm C}(z)]^{7/2}. \tag{3.4}$$

This expression is valid wherever the cloud is Bose condensed[7]. Equating Eqs.(3.4) and (3.3) we obtain an expression for $T_{\rm f}(z)/T_{\rm C}(z)$. This expression is particularly simple for the case $T_0 = T_{\rm C}$ ($D = 1$),

$$\frac{T_{\rm f}(z)}{T_{\rm C}(z)} = \left[\frac{\zeta(5/2)}{\zeta(7/2)}\frac{g_{7/2}[D(z)]}{g_{5/2}[D(z)]}\frac{P_{\rm BE}[7/2,\eta(z),D(z)]}{P_{\rm BE}[5/2,\eta(z),D(z)]}\right]^{2/7}. \tag{3.5}$$

For this special case we calculate $T_{\rm f}(z)/T_{\rm C}(z) < 1$ for $\eta(0) \lesssim 5$, which implies BEC over the *full* length of the cloud where the presumption of local thermalization can be justified.

For the experiments in Amsterdam the degeneracy parameter is $D \approx 0.95$, hence $T_0 > T_{\rm C}$. Numerical calculation shows that in this case the condensate will not nucleate over its full length but still over a region larger than the equilibrium size. This region is indicated by the dotted lines in Fig.4b. In Fig.4a the initial condensate shape is indicated along with the final equilibrium condensate. As the length of the equilibrium condensate is less than the size at nucleation, the cloud will oscillate in shape to reach equilibrium.

The simultaneous condensation over a large region as a result of local thermalization supports the physical picture in which, just after nucleation, there is no phase coherence over distances larger than approximately one mean free path. In such condensates the mean field suppresses density fluctuations but long-range phase coherence is absent. Quasicondensates of this type were put forward in relation to Bose-Einstein condensate formation by Svistunov *et al.* [6,20,21]. Later it was shown that in elongated condensates thermally excited phase fluctuations can persist also under equilibrium conditions [22]. This was demonstrated experimentally in Hannover and Orsay [23,24]. In Amsterdam, it was shown by condensate focusing that 11 ms after nucleation the phase coherence length is still of the order of 1 μm, demonstrating the presence of excess (non-equilibrium) phase fluctuations [5,25].

Acknowledgements

This work is part of the research program on Cold Atoms of the Stichting voor Fundamenteel Onderzoek der Materie (FOM), which is financially supported by the Nederlandse Organisatie voor Wetenschappelijk Onderzoek (NWO).

[6]Note, by substituting $n_1(0) = n_0(\Lambda kT/\hbar\omega_\rho)^2 g_{5/2}[D]/g_{3/2}[D]$, that this procedure yields for the trap center the usual expression for T_C in deep, $\eta(z) \to \infty$, anisotropic harmonic traps.

[7]To arrive at this result we use the property that the thermal fraction of a Bose condensed cloud in a cylindrically symmetric radially harmonic trap is given by $N'/N_{\rm tot} = (T_{\rm f}/T_C)^{5/2}$.

References

[1] Anderson M.H., Ensher J.R., Matthews M.R., Wieman C.E. and Cornell E.A., Science **269** (1995) 198.
[2] Davis K.B., Mewes M.-O., Andrews M.R., van Druten N.J., Durfee D.S., Kurn D.M. and Ketterle W., Phys. Rev. Lett. **75** (1995) 3969.
[3] Miesner H.-J., Stamper-Kurn D.M., Andrews M.R., Durfee D.S., Inouye S. and Ketterle W., Science **279** (1998) 1005.
[4] Köhl M., Davis M.J., Gardiner C.W., Hänsch T.W. and Esslinger T., Phys. Rev. Let. **88** (2002) 80402.
[5] Shvarchuck I., Buggle Ch., Petrov D.S., Dieckmann K., Zielonkowski M., Kemmann M., Tiecke T., von Klitzing W., Shlyapnikov G.V. and Walraven J.T.M., Phys. Rev. Lett. **89** (2002) 270404.
[6] Kagan Yu.M., Svistunov B.V. and Shlyapnikov G.V., Sov. Phys. JETP **75** (1992) 387.
[7] Kagan Yu., Surkov E.L. and Shlyapnikov G.V., Phys. Rev. A **55** (1997) R18-R21.
[8] Griffin A., Wu W.C. and Stringari S., Phys. Rev. Lett. **78** (1997) 1838.
[9] Wu H. and Arimondo E., Europhys. Lett. **43** (1998) 141.
[10] Guéry-Odelin D., Zambelli F., Dalibard J. and Stringari S., Phys. Rev. A **60** (1999) 4851.
[11] Al Khawaja U., Pethick C.J. and Smith H., J. Low Temp. Phys. **118** (2000) 127.
[12] Guéry-Odelin D., Phys. Rev. A **66** (2002) 033613.
[13] Pedri P., Guéry-Odelin D. and Stringari S., Phys. Rev. A **68** (2003) 043608.
[14] Shvarchuck I., Buggle Ch., Petrov D.S., Kemmann M., von Klitzing W., Shlyapnikov G.V. and Walraven J.T.M., Phys. Rev. A **68** (2003) 063603.
[15] Dieckmann K., Spreeuw R.J.C., Weidemüller M. and Walraven J.T.M., Phys. Rev. A **58** (1998) 3891.
[16] Ketterle W., Durfee D.S. and Stamper-Kurn D.M., in Proc. Int. School Phys. *Enrico Fermi* course CXL, M. Inguscio, S. Stringari, C. Wieman (Eds.), IOS Press, Amsterdam (1999).
[17] Chapman S. and Cowling T.G., *The Mathematical Theory of Non-Uniform Gases*, Cambridge University Press, Cambridge 1970.
[18] van Kempen E.G.M., Kokkelmans S.J.J.M.F., Heinzen D.J. and Verhaar B.J. Phys. Rev. Lett. **88** (2002) 93201.
[19] Gardiner C.W., Zoller P., Ballagh R.J. and Davis M.J., Phys. Rev. Lett. **79** (1997) 1793.
[20] Svistunov B.V., J. Mosc. Phys. Soc. **1** (1991) 373.
[21] Berloff N.G. and Svistunov B.V., Phys. Rev. A **66** (2002) 13603.
[22] Petrov D.S., Shlyapnikov G.V. and Walraven J.T.M., Phys. Rev. Lett. **87** (2001) 50404.
[23] Dettmer S., Hellweg D., Ryytty P., Arlt J.J., Ertmer W. and Sengstock K., Petrov D.S. and Shlyapnikov G.V., Kreutzmann H., Santos L. and Lewenstein M., Phys. Rev. Lett. **87** (2001) 160406; App. Phys. B**73** (2001) 1.
[24] Gerbier F., Thywissen J.H., Richard S., Hugbart M., Bouyer P. and Aspect A., Phys. Rev. A **67** (2003) 051602.
[25] Shvarchuck I., Buggle C., Petrov D.S., Kemmann M., Tiecke T.G., von Klitzing W., Shlyapnikov G.V. and Walraven J.T.M., in: Interactions in Ultracold Gases: From Atoms to Molecules, M. Weidemüller & C. Zimmermann (Eds.), J. Wiley, New York (2003)